# Development of an Optimal Variable-Pitch Controller for Floating Axial-Flow Marine Hydrokinetic Turbines

## Preprint

Athul Krishna Sundarrajan,[1] Thanh Toan Tran,[2] Will Wiley,[2] Hannah Ross,[2] Daniel Zalkind,[2] and Daniel R. Herber[1]

*1 Colorado State University*
*2 National Renewable Energy Laboratory*

*Presented at ASME 2024 International Design Engineering Technical Conferences and Computers and Information in Engineering Conference (IDETC/CIE2024)*
*Washington, D.C.*
*August 25–28, 2024*

**NREL is a national laboratory of the U.S. Department of Energy**
**Office of Energy Efficiency & Renewable Energy**
**Operated by the Alliance for Sustainable Energy, LLC**

This report is available at no cost from the National Renewable Energy Laboratory (NREL) at www.nrel.gov/publications.

Contract No. DE-AC36-08GO28308

**Conference Paper**
NREL/CP-5700-89851
June 2024

# Development of an Optimal Variable-Pitch Controller for Floating Axial-Flow Marine Hydrokinetic Turbines

## Preprint

Athul Krishna Sundarrajan,[1] Thanh Toan Tran,[2] Will Wiley,[2] Hannah Ross,[2] Daniel Zalkind,[2] and Daniel R. Herber[1]

*1 Colorado State University*
*2 National Renewable Energy Laboratory*

**Suggested Citation**
Sundarrajan, Athul Krishna, Thanh Toan Tran, Will Wiley, Hannah Ross, Daniel Zalkind, and Daniel R. Herber. 2024. *Development of an Optimal Variable-Pitch Controller for Floating Axial-Flow Marine Hydrokinetic Turbines: Preprint*. Golden, CO: National Renewable Energy Laboratory. NREL/CP-5700-89851. https://www.nrel.gov/docs/fy24osti/89851.pdf.

**NREL is a national laboratory of the U.S. Department of Energy**
**Office of Energy Efficiency & Renewable Energy**
**Operated by the Alliance for Sustainable Energy, LLC**

This report is available at no cost from the National Renewable Energy Laboratory (NREL) at www.nrel.gov/publications.

Contract No. DE-AC36-08GO28308

**Conference Paper**
NREL/CP-5700-89851
June 2024

National Renewable Energy Laboratory
15013 Denver West Parkway
Golden, CO 80401
303-275-3000 • www.nrel.gov

**NOTICE**

This work was authored in part by the National Renewable Energy Laboratory, operated by Alliance for Sustainable Energy, LLC, for the U.S. Department of Energy (DOE) under Contract No. DE-AC36-08GO28308. Funding provided by U.S. Department of Energy Office of Energy Efficiency and Renewable Energy Water Power Technologies Office. The views expressed herein do not necessarily represent the views of the DOE or the U.S. Government. The U.S. Government retains and the publisher, by accepting the article for publication, acknowledges that the U.S. Government retains a nonexclusive, paid-up, irrevocable, worldwide license to publish or reproduce the published form of this work, or allow others to do so, for U.S. Government purposes.



*Cover Photos by Dennis Schroeder: (clockwise, left to right) NREL 51934, NREL 45897, NREL 42160, NREL 45891, NREL 48097, NREL 46526.*

# DEVELOPMENT OF AN OPTIMAL VARIABLE-PITCH CONTROLLER FOR FLOATING AXIAL-FLOW MARINE HYDROKINETIC TURBINES

**Athul Krishna Sundarrajan[1]*, Thanh Toan Tran[2], Will Wiley[2], Hannah Ross[2], Daniel Zalkind[2], Daniel R. Herber[1]**

[1]Department of Systems Engineering
Colorado State University
Fort Collins, CO 80523

[2]National Renewable Energy Laboratory
Golden, CO 80401

## ABSTRACT

*This article discusses the development of an optimal variable-pitch controller for floating, axial-flow marine turbines. Recently, OpenFAST, an open-source wind turbine modeling tool, has been extended to model marine turbines. A controller is necessary to simulate marine turbines for different load cases using OpenFAST, which greatly impacts the performance of the energy system. Previous studies have designed controllers using a linearized model of the marine turbine, which can be time-consuming and require the expertise of a control engineer. In this study, we use an automated approach that uses generic models of the marine turbine to identify the controller gains, which can expedite the process of designing a controller. Using an optimizer to identify the control system parameters can additionally improve the controller's performance. The optimal controller tuned using such an approach results in a* 20% *reduction in the tower-base damage equivalent loading and better tracking of the rated generator speed and power.*

## 1 INTRODUCTION

There has been rising interest in using marine turbines to harvest the energy present in tidal currents [1, 2]. Similar to how wind turbines convert the kinetic energy in the wind, marine turbines convert the kinetic energy of flowing water in tidal or riverine environments to electrical energy. A recent study has estimated that 2300 TWh/yr of energy is available from tidal and riverine currents in the United States [3]. A significant portion of this energy is located in remote locations like Alaska and Hawaii. By harvesting the energy available in tidal and riverine currents, it is possible to reduce the use of fossil fuels to generate electricity in these locations [4]. A major impediment to the widespread adoption of marine turbines is the current high cost of energy [1, 5]. Several factors impact the cost of energy, including the physical design, manufacturing, installation, and maintenance costs of marine turbines, and the controller [1, 6]. In this article, we restrict our focus to the controller and investigate how the controller and its design can impact the turbine's performance. Due to the dynamic and stochastic nature of the tidal/riverine environment, a controller is necessary to extract maximum power and reduce the loads over the entire range of current and wave inputs. To find system-optimal designs, it is important to take into account the effect the controller has on the performance of marine turbines in early-stage design studies [1, 5].

Identifying cost-optimal designs will help the wide-scale adoption of marine energy technologies [7]. Exploring multiple designs and comparing their performance can help designers and manufacturers understand the underlying design trade-offs and identify an optimal design that balances multiple considerations. The current modeling and design practices utilized

*Corresponding author, athul.sundarrajan@colostate.edu

for marine turbines do not facilitate efficient design space exploration [8–11].

Typically, a lower-order model is developed for a specific design to get an estimate of its loads and performance [8–11]. In parallel, scaled experimental models are fabricated and tested for these specific designs when feasible [10–14]. These studies provide critical insights into the performance of specific concepts. However, it is unclear if these models and experimental setups can be easily extended to other designs and architectures. The availability of open-source modeling and design tools can expedite the process of identifying a standard architecture by helping researchers explore the feasibility and characterize the performance of various designs [6].

### 1.1 Controller Design and Tuning

The choice of the control scheme has a significant impact on the design and performance of the marine turbine. Regardless of the control scheme, traditional wind turbine operating regions, control goals, variables, and tuning processes have been adopted for marine turbines as well [15]. The two main control variables in both applications are the blade pitch ($\beta$) and the generator torque ($\tau_g$). Based on these variables, the two control schemes that are considered for marine turbines are fixed-pitch variable-speed (FP-VS) control and variable-pitch variable-speed control (VP-VS). Predominantly, an FP-VS scheme has been utilized for marine turbines to keep the design simple and reduce the risk of failure associated with a blade pitch mechanism. However, despite similar concerns, the benefits of using a blade pitch mechanism in minimizing the loads and increasing the power production have led to their widespread adoption for wind turbines [16].

Similar to the control of wind turbines, the generator speed ($\omega_g$) is the main feedback variable for marine turbines. The system is linearized around set operating points for both VP-VS and FP-VS schemes, and controllers are designed through Bode-shaping [17]. Additional parameters also characterize the controller's performance. The values of the parameters are selected to give a "reasonable" performance. Such an approach has a number of drawbacks that make it unsuitable for early-stage design exploration studies. First, if the turbine's physical design changes, the tuning process must be repeated to design a controller for that specific turbine design realization. Deriving linearized models of the system can be computationally expensive, and the expertise of a control engineer is required to select good values for the control gains [18].

Additionally, to test the performance of the design and the controller, the marine turbine must be simulated over a wide range of design load cases (DLCs) specified by the International Electrotechnical Commission (IEC) [19, 20]. For the design to have a lower levelized cost of energy (LCOE), the controller must be able to generate the rated power for the turbine and minimize loads over the entire range of DLCs. A controller tuned to have a "reasonable" performance cannot meet such requirements. The design space for the controller parameters can be nonlinear. Therefore, finding the optimal parameters is often nonintuitive. Recently, optimization studies have been used to design controllers that can satisfy these challenging requirements [19, 21]. To explore the design space more efficiently, a controller that can be modified easily and be used in conjunction with an optimizer is necessary.

### 1.2 Using OpenFAST for Modeling Marine Turbines

OpenFAST, an open-source modeling tool for horizontal-axis wind turbines developed by the National Renewable Energy Laboratory (NREL), has been widely adopted to explore the associated design space of wind turbines and establish their performance. Recent updates made to OpenFAST enable the simulation of marine turbines [22]. Additionally, the Reference Open-Source Controller (ROSCO), introduced in Ref. [23], is an open-source controller for wind turbines that has an automated tuning process while providing industry-standard functionalities. ROSCO uses a generic model of a given turbine to schedule gains for both the torque and blade pitch controllers. The controller and the gains are parameterized by additional variables that can be specified by the user or identified using an optimizer. These features make ROSCO an ideal tool to be used in early-stage design studies.

The goal of this article is to extend ROSCO for the control of marine turbines and demonstrate the benefits of using an optimizer to identify the optimal design of the controller. The system under consideration is described in Ref. [24] and is based on an open-source marine turbine model first introduced in Refs. [2, 7]. The rest of the article is organized as follows. Section 2 provides a brief overview of the two different control frameworks that are common in marine turbines. Section 3 provides an overview of the changes made to OpenFAST to model the dynamics of marine turbines and a brief description of the open-source marine turbine model used in this article. Section 4 provides an overview of ROSCO, and Sec. 5 details the formulation of the control optimization problem. Section 6 discusses the performance of the optimal controller for the baseline Reference Model 1 (RM1) turbine. In Sec. 7, we summarize the study and provide directions for future work.

## 2 MARINE TURBINE CONTROL FRAMEWORKS

For marine turbines, similar to wind turbines, the inflow speed is divided into below-rated and above-rated regions, and different control goals are utilized in each region [15]. In the below-rated region, generator torque ($\tau_g$) is the primary control variable [17, 25]. In the above-rated region, two different control strategies are possible [26].

### 2.1 Fixed-Pitch Control

In FP-VS turbines, the blades are fixed to the nacelle at an optimal angle, and $\tau_g$ is varied to track the rated power. The lack of a pitching mechanism reduces the capital and maintenance costs and keeps the overall design simple [27]. There are, again, two different ways fixed-pitch controllers can track the rated power, namely, overspeed control or underspeed control [28]. In the overspeed control strategy, generator speed ($\omega_g$) is increased by reducing the generator torque [29, 30]. In underspeed control, $\tau_g$ is increased to lower $\omega_g$ and track the rated power [31].

Despite allowing a simpler design, FP-VS turbines have several drawbacks. Since larger values of $\tau_g$ are required in underspeed control, the size of the generator must be increased [28]. As the target $\omega_g$ varies with the current input, there is a larger fluctuation in the power generated [15]. Furthermore, the blades for underspeed turbines are specifically designed to induce stall at higher flow speeds [15, 28, 31, 32]. Because of these issues, the efficiency of fixed-pitch turbines is comparatively lower than their variable-pitch counterparts, and the blades must be designed to withstand higher loads.

### 2.2 Variable-Pitch Control

For VP-VS turbines, in the above-rated region, the blade pitch is varied to keep the turbine rotating at its rated speed [17, 26]. The addition of the blade pitch mechanism increases the capital cost and modes of failure, which subsequently increases the risk of downtime and maintenance costs [28]. However, using blade pitch control results in lower thrust and fatigue loads and better power tracking compared to fixed-pitch controllers [25]. Additionally, as the turbine size increases, the ability of the blade pitch mechanism to reduce the increased loads on the system becomes critical [16]. Therefore, the focus of this article will be on VP-VS turbines.

## 3 BASELINE MARINE TURBINE MODEL

There are a limited number of open-source tools that are capable of modeling marine turbines. Recently, the open-source wind turbine modeling tool OpenFAST has been extended to support the simulation of axial-flow marine turbines and is available at Ref. [33]. The addition of buoyant forces on the blade sections, hub, nacelle, and tower and the ability to model turbines below sea level enables the use of OpenFAST to model marine turbines. These new features can help marine energy developers, including industry and academia, better predict marine turbine performance and loads as well as advance this technology space through control co-design optimization [6].

In this study, a baseline model called the Floating RM1 Quad (F-RM1-Q), introduced in Ref. [24] and shown in Fig. 1, is used to demonstrate the new capabilities of the open-source ROSCO controller. This model is based on the RM1 turbine, introduced in Refs. [2, 7]. The RM1 model discussed in Refs. [2, 7] has a twin-rotor configuration that is fixed to the sea bottom. OpenFAST currently does not have the ability to model a twin-rotor system. Therefore, the F-RM1-Q only includes one rotor. The model was designed by NREL such that new features added to the OpenFAST code can be tested and demonstrated. The supporting structure for the F-RM1-Q is an asymmetric semisubmersible platform. It consists of four main columns that are connected by a series of smaller-diameter cross members. Heave plates are attached to the bottom of the main columns and serve to dampen platform motion. The rotor-nacelle assembly (RNA) is connected to the center of the platform via a supporting structure (i.e., tower). The physical rotor system designed in Refs. [2, 7] is used with this platform. The mooring system is also asymmetric, providing the large surge stiffness needed to counter the turbine thrust with six catenary lines. Details of the F-RM1-Q specifications can be found in Ref. [24].

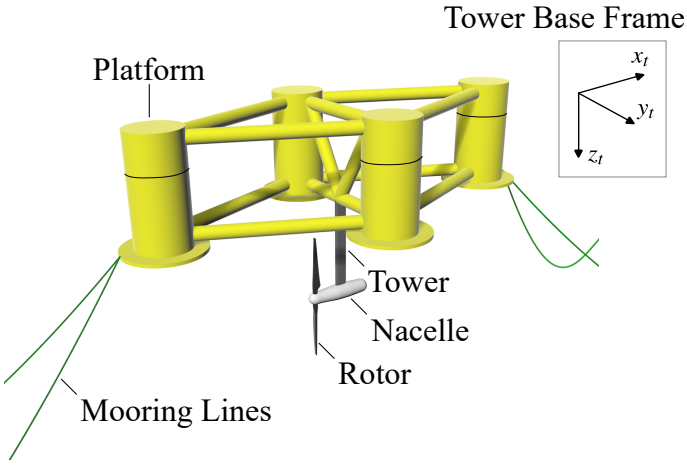


**FIGURE 1**: RM1 Quad (illustration courtesy of NREL).

## 4 ROSCO

### 4.1 ROSCO Overview

ROSCO is a reference open-source controller developed by NREL for the control of fixed and floating wind turbines [23] and is available at Ref. [34]. ROSCO uses a simplified, first-order model along with the $C_p$ surface of the given turbine to estimate how $\omega_g$ varies with the two primary control variables $\tau_g$ and $\beta$:

$$\dot{\omega}_g = \frac{N_g}{J}\left(\tau_a - N_g \tau_g \eta_{\text{gb}}\right) \tag{1a}$$

$$\tau_a = \frac{1}{2}\rho A_r \frac{C_p(\lambda,\beta)}{\omega_r} v^3 \tag{1b}$$

where $N_g$ is the gearbox ratio, $A_r = \pi R^2$ is the swept area and $R$ is the radius of the blades, $v$ is the current (or wind) speed, $J$ is the rotor inertia, $\rho$ is the density of the fluid, $\eta_{\text{gb}}$ is the combined

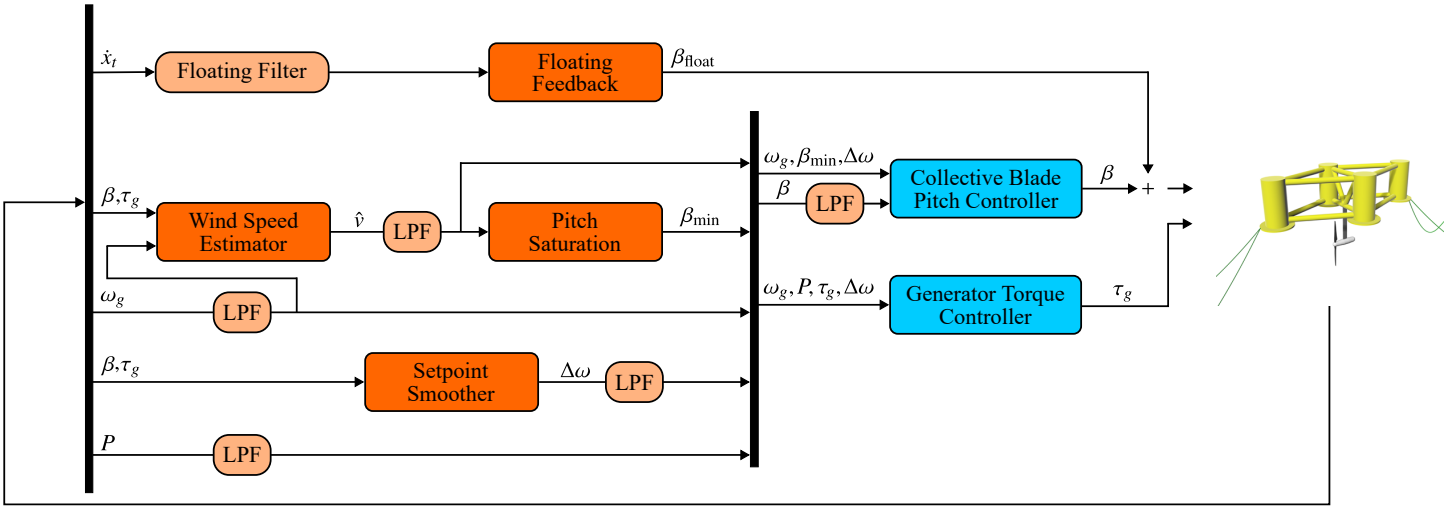


**FIGURE 2**: A block diagram summarizing the key components of the ROSCO toolbox. The main feedback variables are the generated power ($P$), the generator speed ($\omega_g$), and the tower-top velocity ($\dot{x}_t$). The generator torque controller is summarized in Sec. 4.2, and the blade pitch controller and the floating feedback are summarized in Sec. 4.3.

generator and gearbox efficiency, $C_p$ is the power coefficient expressed as a function of $\beta$ and the tip speed ratio ($\lambda$), and $\omega_r$ and $\tau_a$ are the rotor speed and aerodynamic torque, respectively. Let $\boldsymbol{X}$ denote the variables associated with Eqs. (1a) and (1b):

$$\boldsymbol{X} = \left[N_g, J, \tau_a, \eta_{\text{gb}}, \rho, A_r, C_p, \omega_r, \lambda\right] \tag{2}$$

Equations (1a) and (1b) can be used to describe certain aspects of the RM1 turbine given in Sec. 3. Additionally, the RM1 turbine is designed to have a variable-pitch controller in the above-rated region. Therefore, ROSCO can be used to develop the necessary controllers for the RM1 turbine.

Two different control loops, both using a reference tracking proportional-integral (PI) architecture, are developed for $\tau_g$ (for the below-rated region) and $\beta$ (for the above-rated region). The generator speed ($\omega_g$) is the main feedback variable for both control loops. A set-point smoother is used to provide a smooth transition between these two controllers in the near-rated region ($\sim$ 2.0 m/s). The closed-loop system for both controllers and the corresponding proportional ($\boldsymbol{k}_p$) and integral ($\boldsymbol{k}_i$) gain schedules are derived using first-order linearizations of Eqs. (1a) and (1b). A block diagram of the ROSCO controller is shown in Fig. 2.

The input to this closed-loop system is the generator speed error, measured as:

$$-\Delta\omega_g = \omega_{g,\text{ref}} - \omega_g \tag{3}$$

where $\omega_{g,\text{ref}}$ is the reference generator speed, and the output is the control response $\Delta\tau_g$ or $\Delta\beta$. The resulting closed-loop system between $\Delta\tau_g$ or $\Delta\beta$ and $\Delta\omega_g$ is a second-order system with a response characterized by its natural frequency ($\omega_{\text{des}}$) and damping ratio ($\zeta_{\text{des}}$) [35]. The gains $\boldsymbol{k}_p$ and $\boldsymbol{k}_i$ for both the control systems subsequently depend on $\boldsymbol{p} = [\omega_{\text{des}}, \zeta_{\text{des}}]$ and the variables in $\boldsymbol{X}$. Briefly, $\omega_{\text{des}}$ affects how quickly the controller can respond to a change in the reference, and $\zeta_{\text{des}}$ affects the oscillatory response of the system. The desired controller performance can be achieved by selecting the appropriate values of $\boldsymbol{p}$. Please refer to Ref. [23] for a thorough discussion of the control loops and the tuning process. Sections 4.2 and 4.3 provide a brief overview of the $\omega_{g,\text{ref}}$ used for the below- and above-rated controllers and their associated gains.

### 4.2 Below-Rated Generator Torque Control

The generator torque is the main control variable used in the below-rated region. A commonly used control goal in the below-rated region is to track the $\omega_{g,\text{ref}}$ value that keeps the turbine operating at its optimal tip-speed ratio, $\lambda_{\text{opt}}$:

$$\omega_{g,\text{ref}} = N_g \frac{\lambda_{\text{opt}} \hat{v}}{R} \tag{4}$$

where $\hat{v}$ is the estimated rotor-effective current speed. Current speeds cannot be accurately measured at the turbine, so an estimator is required. Modeling uncertainties can lead to biases in the current speed estimate. To remove the speed estimator from the control loop, we use a new $\omega_{g,\text{ref}}$ value that can be obtained as follows from the relations for power generated ($P$) and $\tau_g$, discussed in Refs. [16, 23]:

$$\tau_g = K\omega_g^2 \quad \text{and} \quad \tau_g = \frac{P}{\omega_g} \tag{5}$$

Equating these two, we get:

$$\omega_{g,\text{ref}} = \omega_g = \left[\frac{P}{K}\right]^{\frac{1}{3}} \tag{6}$$

where $K$ is given by:

$$K = \frac{1}{2}\rho\pi R^5 \frac{C_{p,\max}}{\lambda_{\text{opt}}} \frac{1}{N_g^3 \eta_{\text{gb}}} \tag{7}$$

This reference does not depend on $\hat{v}$ and doesn't adversely affect the performance obtained using Eq. (4). As shown in Fig. 2, the generator power signal is passed through a low-pass filter, before being used to calculate $\omega_{g,\text{ref}}$. The values of $\omega_{\text{vs}}$ and $\zeta_{\text{vs}}$[1] are then selected as $\boldsymbol{p}_{\text{vs}} = [0.7, 0.7]$ to derive $\boldsymbol{k}_{p,\text{vs}}$ and $\boldsymbol{k}_{i,\text{vs}}$. As opposed to a gain schedule for $\boldsymbol{k}_{p,\text{vs}}$ and $\boldsymbol{k}_{i,\text{vs}}$ for different values $v$, the values corresponding to the rated flow speed $v = v_{\text{rated}}$ are used to simplify controller implementation without affecting the performance.

### 4.3 Above-Rated Blade Pitch Control

The control goal in the above-rated region is to vary $\beta$ to track the rated generator speed $\omega_{g,\text{ref}} = \omega_{g,\text{rated}}$ for the turbine. Similar to the below-rated controller, $\omega_{\text{pc}}$ and $\zeta_{\text{pc}}$ are selected to derive the corresponding gains $\boldsymbol{k}_{p,\text{pc}}$ and $\boldsymbol{k}_{i,\text{pc}}$. The performance of the turbine in the above-rated region is critical because the majority of the power is generated in this region, and, correspondingly, the loads on the turbine are higher. Subsequently, the performance of the blade pitch controller must be optimized to meet the design goals. To improve the performance of the blade pitch controller, multiple values of $\boldsymbol{\omega}_{\text{pc}}$ and $\boldsymbol{\zeta}_{\text{pc}}$ for different values of $\boldsymbol{v}$ can be selected [21]. In addition to this control loop, for floating turbines, a feedback term is included to address the "negative-damping" problem.

**Negative-damping problem.** The negative-damping problem is a known issue for floating turbines that use blade pitch control in the above-rated region [32, 36, 37]. Briefly, this phenomenon occurs as a result of the coupling between the tower motion and the blade pitch. Consider the case when the turbine is pitching forward. This forward motion increases the relative current speed faced by the turbine, thereby increasing the generator/rotor speed. The blade pitch controller then seeks to keep the generator speed at its rated value. When the response of the blade pitch controller ($\omega_{\text{pc}}$) is faster than the tower motion ($\omega_{\text{tower}}$), the relative thrust experienced by the turbine is reduced, causing the turbine to pitch forward even more, and vice versa when the turbine is pitching backward. This causes the tower fore-aft and platform pitching motion to be undamped. This subsequently increases the tower-base loads and affects $\omega_g$ regulation. To counteract this, the tower-top velocity ($\dot{x}_t$) is filtered and proportionally fed back to the blade pitch controller to dampen the pitching motion. A combination of first-order high-pass, second-order low-pass, and notch filters is applied to the tower-top velocity signal. The corner frequencies of the high-pass and low-pass filters are at 0.01 rad/s and the fore-aft natural frequency of the platform $\omega_{\text{ptfm}}$, respectively. The corresponding proportional gain is represented by $k_{\beta,\text{float}}$. This gain can either be derived using a generic tuning procedure in ROSCO or can be specified by the user.

In addition to these control loops, ROSCO has a number of modules and filters that provide additional functionalities. The reader can refer to Refs. [16, 23] for a detailed overview of the first-order model, tuning procedure, and the additional modules used in ROSCO.

## 5 CONTROLLER OPTIMIZATION

We focus here on optimizing the performance of the system by tuning the blade pitch controller. The performance of the blade pitch controller is characterized by the variables $\boldsymbol{p}_u = [\boldsymbol{\omega}_{\text{pc}}, \boldsymbol{\zeta}_{\text{pc}}, k_{\beta,\text{float}}, \omega_{\text{ptfm}}]$. Therefore, $\boldsymbol{p}_u$ is selected as the set of optimization variables used in this study. The gains $\boldsymbol{\omega}_{\text{pc}}$ and $\boldsymbol{\zeta}_{\text{pc}}$ for two different values of $v$, one in the near-rated region and one for the above-rated region at $\boldsymbol{v} = [2.0, 2.7]$ m/s are chosen.

For the purposes of this study, the turbine will be simulated using environmental data from Cook Inlet off the coast of Alaska. The metocean (meteorological-oceanographic) conditions are obtained from the study carried out in Ref. [38]. We simulate the model in OpenFAST using 11 different current profiles characterized by the average current speed ($v_{\text{avg}}$) with $v_{\text{avg}} \in [0.5, 3]$ m/s and use the results from the simulations to calculate the fatigue loads, power production, and other quantities. In the rest of the article, one function evaluation implies that the turbine is simulated for these 11 load cases. The turbulence intensity TI [%], which is the ratio of the standard deviation of $v$ to the mean for all 11 load cases, is shown in Fig. 3a. The probability distribution for $v$ at this location is also shown in Fig. 3b. In addition to the current, the turbine is subjected to irregular waves generated from the JONSWAP spectrum for different significant wave heights $H_s$ [m] and significant wave periods $T_p$ [s] as shown in Fig. 3a. Different $H_s$ and $T_p$ are used for each of the 11 load cases.

The optimal controller would help in balancing the power production and minimizing the ultimate and fatigue loads on the turbine. The IEC TS 62600-2 specifies that both the ultimate and fatigue loads must be calculated to assess the performance of the turbine [20]. But in this study, we limit our focus to fatigue loads. Studies on floating wind turbines have reported increased tower-base fatigue damage caused by the additional wave loading [39]. To understand this effect for marine turbines, the tower-base fatigue loading will be the key load investigated in the subsequent control design study.

### 5.1 Damage Equivalent Load

In this article, we use the damage equivalent load (DEL) metric to characterize the fatigue load on the turbine. DEL approximates

[1] Where the subscript "vs" refers to variable speed torque control, and subsequently, "pc" refers to pitch control.

the cumulative fatigue damage incurred over a given time span to a single equivalent load that would cause the same damage. This aspect allows the use of DEL as an objective or constraint in the optimization study. We use the rainflow cycle counting method and the Palmgren-Miner rule to estimate the DEL from the time series signals of the tower-base moments. More details regarding the rainflow cycle counting method can be found in Ref. [40]. OpenFAST calculates the tower-base forces and moments in three directions: side-to-side, fore-aft, and yaw. The corresponding moments in each direction are represented as $\mathrm{M}_{t,x}$, $\mathrm{M}_{t,y}$, and $\mathrm{M}_{t,z}$, respectively. The total tower-base moment ($\mathrm{M}_t$) from each load case is calculated from these signals as:

$$\mathrm{M}_t = \sqrt{\mathrm{M}_{t,x}^2 + \mathrm{M}_{t,y}^2 + \mathrm{M}_{t,z}^2} \tag{8}$$

Once the time series signal for $\mathrm{M}_t$ is available, the rainflow counting method is used to identify the loading cycles in the time series. Next, the amplitude and mean moment for every loading cycle is identified. This step provides a range of values for the amplitude and moment corresponding to different loading cycles. This range of amplitudes for the different cycles is then separated into various bins, and the count for each bin is then calculated to obtain the corresponding $\mathrm{M}_{t,i}$ and $n_i$ pair, where $\mathrm{M}_{t,i}$ refers to the amplitude of the "$i$-th" bin, and $n_i$ refers to its count. For a more detailed explanation of how DEL is calculated, please refer to Refs. [39, 41, 42]. Here, 100 bins are used in the calculation of the DEL. The DEL for a specific load case is then calculated as:

$$\mathrm{DEL} = \left( \sum_{i=1}^{100} \frac{M_{t,i}^m n_i}{t_{\mathrm{span}}} \right)^{1/m} \tag{9}$$

where $t_{\mathrm{span}}$ refers to the time span of the time series, and $m = 4$ refers to the slope of the M-N curve for the material. The DEL for all 11 load cases is calculated using the aforementioned steps, and the results are combined to calculate the total tower-base damage equivalent load ($\mathrm{DEL}_t$) as:

$$\mathrm{DEL}_t = \int_v \mathrm{DEL}(v_{\mathrm{avg}}) f_p(v_{\mathrm{avg}}) dv \tag{10}$$

where $\mathrm{DEL}(v_{\mathrm{avg}})$ is DEL for a load case, and $f_p(v_{\mathrm{avg}})$ is the probability of $v_{\mathrm{avg}}$ obtained from the probability distribution shown in Fig. 3b.

Minimizing DEL is chosen as the objective for the control design problem investigated in this article. Other objectives that could be used are discussed briefly in Ref. [21]. A constraint is added to ensure $\omega_g$ does not exceed 20% of its rated value. The resulting optimization problem formulation is:

$$\underset{\boldsymbol{p}_u}{\text{minimize:}} \quad \mathrm{DEL}_t \tag{11a}$$

$$\text{subject to:} \quad \omega_g \leq 1.2 \cdot \omega_{g,\mathrm{rated}} \tag{11b}$$

$$\boldsymbol{p}_{u,\min} \leq \boldsymbol{p}_u \leq \boldsymbol{p}_{u,\max} \tag{11c}$$

where $\boldsymbol{p}_{u,\min} = [0.1, 0.1, -2, 10^{-5}]$ and $\boldsymbol{p}_{u,\max} = [1.5, 3.0, 0.0, 1.0]$, respectively.

In theory, maximizing AEP could also be considered in the objective. Similar to the DEL, the AEP is calculated as:

$$\mathrm{AEP} = 8760 \int_v \bar{P}(v_{\mathrm{avg}}) f_p(v_{\mathrm{avg}}) dv \tag{12}$$

where $\bar{P}$ refers to the average power generated for a load case with a mean of $v_o$. However, for the choice of $\boldsymbol{p}_u$ and its range considered in this article, the AEP does not vary by much from its nominal value. The generator power $P$ is calculated as $P = \tau_g \omega_g$, and the goal of the controller in the above-rated region is to track $\omega_{g,\mathrm{rated}}$ as $\tau_g$ is held constant. From Eq. (12), it is clear that to increase AEP, $\bar{P}$ must be increased. To increase $\bar{P}$, $\omega_{g,\mathrm{rated}}$ must be increased. Since $\omega_{g,\mathrm{rated}}$ is not changed in this study, $\bar{P}$ and, subsequently, the AEP are not affected in a significant manner.

### 5.2 Notes on Computational Time

All the simulations in this article were run on a high-performance computing cluster with 2 x Intel Xeon Gold 6148 CPU with 40 cores per node and 192 GB of RAM. The IEC TS 62600-2 recommends using simulations that are 600 s long to evaluate the performance of the turbine [20]. The standard also recommends that key metrics be evaluated using the turbine's performance for multiple DLCs (1.1, 1.2, 1.3, etc.). Running all 11 load cases considered in this study (i.e., one function evaluation, in parallel) for a time span of 600 s takes approximately 4.5 hours. Depending on the choice of the optimization algorithm, several hundred function evaluations might be required. The computational expense of simulating the system for 600 s for multiple DLCs per the IEC recommendation can be computationally intractable. Therefore, to reduce the computational expense, we simulate the system for a time span of 200 s, which takes approximately 1.3 hours per function evaluation. Additionally, we only use load cases from DLC 1.1 to test the turbine's performance at this time, but with more resources, additional DLCs and longer time spans can be selected.

Based on the recommendation provided in Ref. [21] on the choice of the optimizer, a derivative-free optimizer `COBYLA` introduced in Ref. [43] is used. For every iteration of the optimization problem, the model is simulated for the entire range of DLCs, and the relevant quantities are then calculated from these simulations. The WEIS toolbox, available at Ref. [44], is used to run the studies.

## 6 RESULTS

### 6.1 Baseline Performance

Before discussing the results of the optimization study, it is necessary to validate the control response obtained using ROSCO for the F-RM1-Q turbine. The results reported in Ref. [2] are the only other control-related results for the RM1 turbine available in the literature. Comparing the performance obtained using ROSCO to the results presented in Ref. [2] would be a good approach to validate the control scheme obtained using ROSCO. However, there are certain caveats that must be established be-

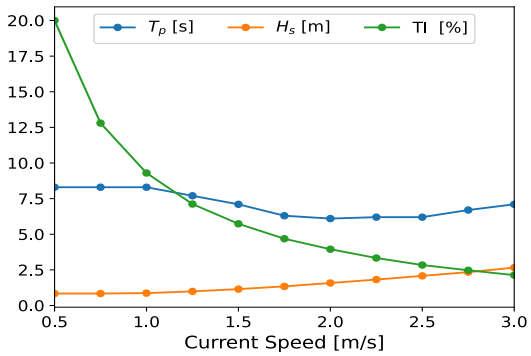


(a) Wave period ($T_p$) [s], wave height ($H_s$) [m], and turbulence intensity (TI ) [%].

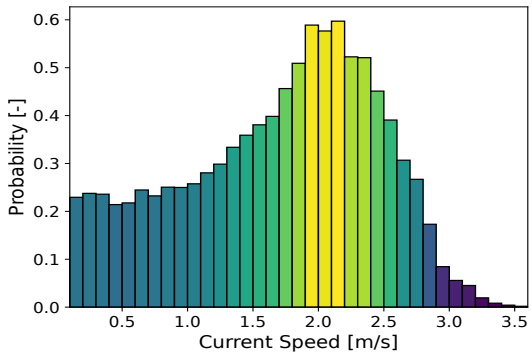


(b) Probability density of the current speed at Cook Inlet.

**FIGURE 3**: The metocean conditions and the probability density of the current speed at Cook Inlet, used to simulate the system in the optimization problem in Eq. (11).

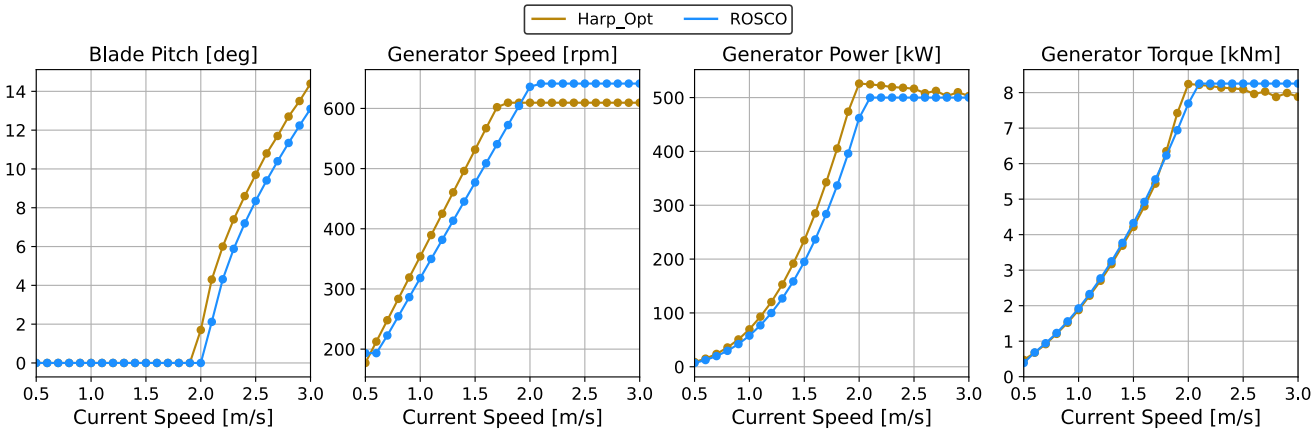


**FIGURE 4**: Comparison of steady-state values of key signals obtained using `Harp_Opt` as reported in Ref. [2] and ROSCO with $\boldsymbol{p}_u = \boldsymbol{p}_{u,\text{init}}$.

fore such a comparison is carried out. The results presented in Ref. [2] are for a fixed configuration of the RM1 turbine. The steady-state values of $\beta$, $\tau_g$, and the resulting $\omega_g$ and $P$ reported in Ref. [2] were identified using a turbine design tool `Harp_Opt`. Therefore, for a fair comparison, the floating degrees of freedom (surge, sway, heave, roll, pitch, yaw) for the F-RM1-Q model are disabled in OpenFAST for this validation study only. The F-RM1-Q turbine is then simulated using constant current speeds for $v \in [0.5, 3]$ m/s, and the steady-state values of $\beta, \tau_g, \omega_g$ and $P$ obtained using ROSCO are plotted against the values reported using `Harp_Opt` in Fig. 4. It is clear from Fig. 4 that the trends and values of $\beta, \tau_g, \omega_g$, and $P$ obtained using ROSCO are similar to the values reported in Ref. [2]. The difference in the steady-state values can be attributed to the different control goals and methodologies used by these two approaches.

With the control trends validated, we simulated the F-RM1-Q model using $\boldsymbol{p}_{u,\text{init}}$ for the load cases described in Sec. 5, with the floating degrees of freedom enabled. The time series plots of some key signals for three different current speeds in the below-rated, transition, and above-rated regions are shown in Fig. 5. Figure 5a shows how the control variables $\tau_g$ and $\beta$ change in different regions. In the below-rated region, $\tau_g$ is the main control variable. Similarly, $\beta$ is the main control variable in the above-rated region, and $\tau_g$ is held constant. In the transition region, a combination of these two variables is used. These control trajectories obtained by using the goals outlined in Sec. 4 are in line with the trends seen for wind turbines. The $\text{DEL}_t$ calculated over the range of DLCs when using $\boldsymbol{p}_{u,\text{init}}$ is 1327.89 kNm as shown in Table. 1. The rotor overspeed value is 35.40 %. The performance of the controller can be improved by using an optimizer to find values of $\boldsymbol{p}_u$.

## 6.2 Optimization Results

The optimization problem is solved using $\boldsymbol{p}_{u,\text{init}}$ as the initial value with an optimality tolerance of $o = 10^{-2}$. The optimizer converges to a point with a lower objective value that satisfies

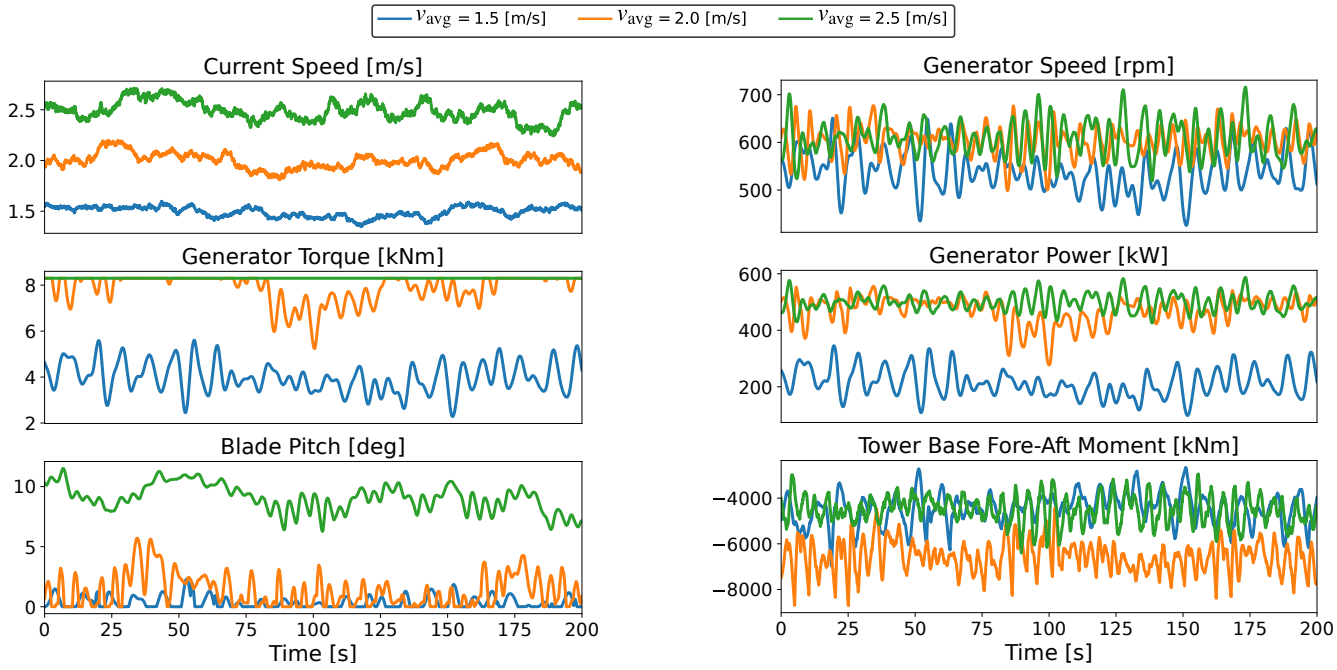


(a) Current speed and control variables.

(b) Key generator outputs and tower-base fore-aft moment.

**FIGURE 5**: Time series plot of key signals in the below-rated (1.5 m/s), transition (2.0 m/s), and above-rated (2.5 m/s) regions obtained using $\boldsymbol{p}_{u,\text{init}}$.

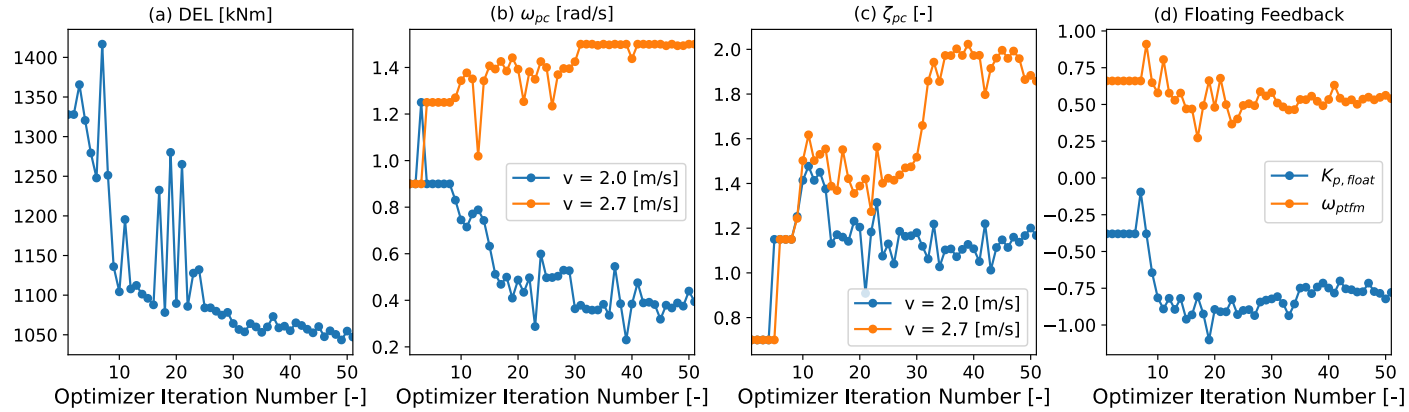


**FIGURE 6**: Convergence of the objective and variables for the optimization problem in Eq. (11) with (a) the objective tower-base damage equivalent loading ($DEL_t$); (b) natural frequency ($\boldsymbol{\omega}_{\text{pc}}$); (c) damping ratio ($\boldsymbol{\zeta}_{\text{pc}}$); and (d) the proportional gain ($K_{p,\text{float}}$) and the bandwidth of the low-pass filter ($\omega_{\text{ptfm}}$) used in the floating feedback controller.

the constraints in 51 iterations. It takes a total of 74 hours to solve the optimization on the high-performance computing cluster mentioned in Sec. 5.2. The optimal values of $\boldsymbol{p}_u$ denoted by $\boldsymbol{p}_{u,\text{opt}}$ and the objective function $\text{DEL}_t$ are presented in Table 1. The final value of $\text{DEL}_t$ is 1052.01 kNm, which represents a 20.77% reduction from the unoptimized value. The optimal point identified by the optimizer also reduces the rotor overspeed to 19.5%, which satisfies the constraint placed in Eq. (11). The convergence of $\text{DEL}_t$ and $\boldsymbol{p}_u$ are shown in Fig. 6.

Of the signals used to calculate $\text{M}_t$ in Eq. (8), the tower-base fore-aft moment ($\text{M}_{t,y}$) is the key driver for this system. By understanding how $\text{M}_{t,y}$ changes for $\boldsymbol{p}_{u,\text{init}}$ and $\boldsymbol{p}_{u,\text{opt}}$, we can understand the results of this optimization study. To minimize $\text{DEL}_t$, it is necessary to minimize the amplitude of the loading cycles in $\text{M}_{t,y}$, which subsequently minimizes $\text{M}_i$ in Eq. (9). The rotor thrust is a key driver for $\text{M}_{t,y}$. The rotor thrust is the force caused

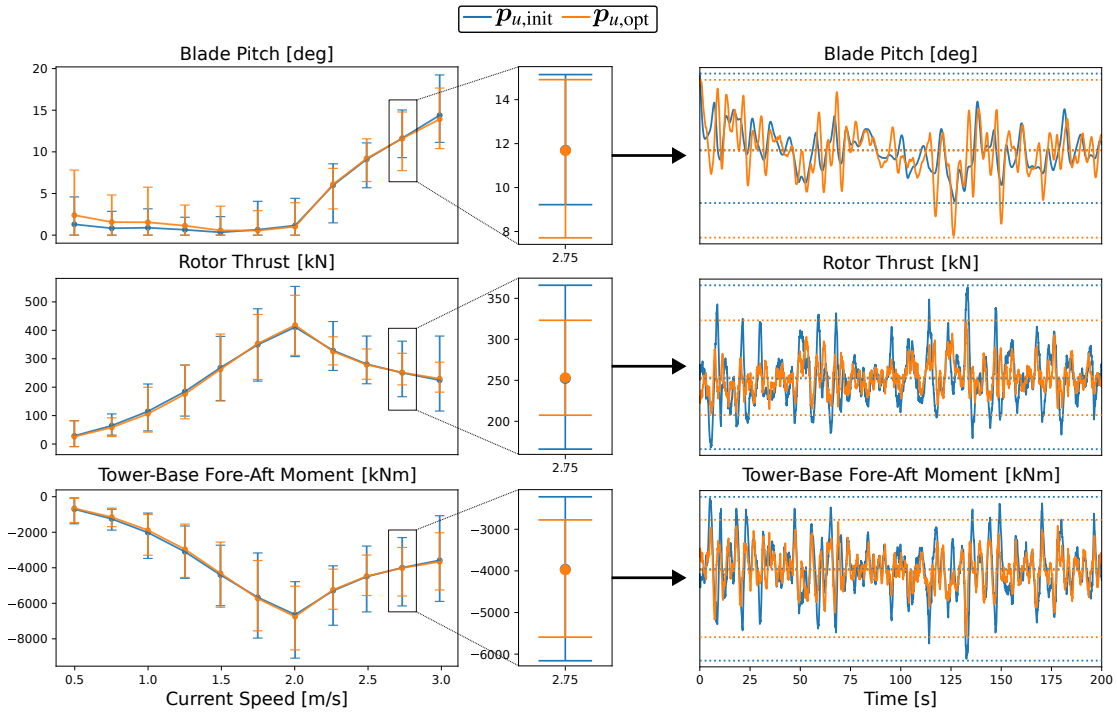


(a) Comparison of the mean values and range of key variables and time series signals for $v_{\text{avg}} = 2.75$ m/s.

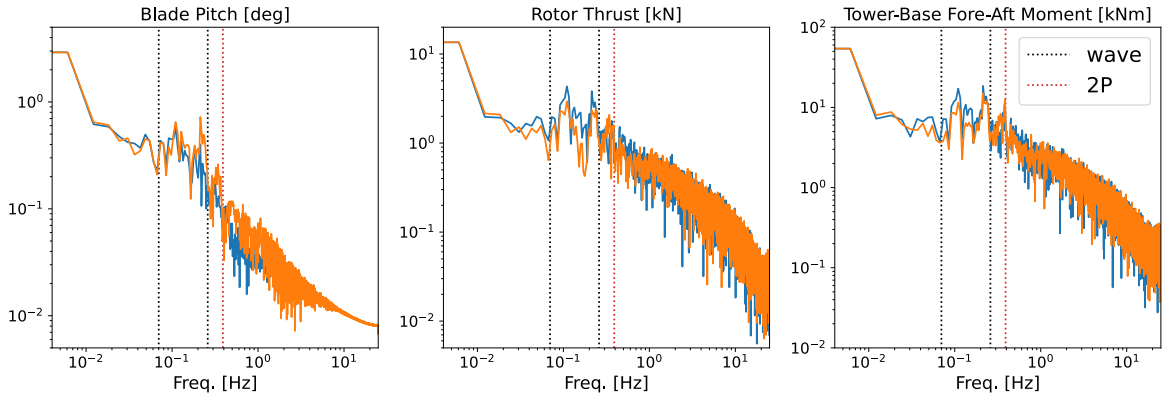


(b) Power spectral density plots of the key signals for $v_{\text{avg}} = 2.75$ m/s.

**FIGURE 7**: Comparison of the mean values of key signals like the blade pitch ($\beta$), rotor thrust, and the tower-base fore-aft moment ($M_{t,y}$) between $\boldsymbol{p}_{u,\text{init}}$ and $\boldsymbol{p}_{u,\text{opt}}$ for all 11 load cases, and the time series of the same quantities for $v_{\text{avg}} = 2.75$ m/s.

by the current flow on the rotor. This force causes a moment at the base of the tower, which is a key driver for $M_{t,y}$. By minimizing the amplitude of fluctuations in the rotor thrust signal, it is possible to minimize the amplitude of loading cycles in $M_{t,y}$.

The mean value and range of key quantities like $\beta$, $M_{t,y}$, and the rotor thrust are plotted in Fig. 7 with $\boldsymbol{p}_{u,\text{init}}$ and $\boldsymbol{p}_{u,\text{opt}}$ for all 11 load cases. It is clear from Fig. 7a, that $\boldsymbol{p}_{u,\text{opt}}$ results in $\beta$ that minimizes the fluctuations in the rotor thrust and subsequently $M_{t,y}$. The oscillations in these three quantities are caused by the wave inputs and the 2P or the "twice per revolution" frequency, which corresponds to the frequency at which the rotor blades cross the tower, as shown by the power spectral density plots in Fig. 7b. Figure 8a shows the time series plot for $M_t$, and Fig. 8b shows the histogram of the amplitudes for different cycles obtained using the rainflow counting method for a load case with $v_{\text{avg}} = 2.75$ m/s for both $\boldsymbol{p}_{u,\text{init}}$ and $\boldsymbol{p}_{u,\text{opt}}$. In Fig. 8b, we use $n = 10$ bins to visualize the reduction in amplitude better, but $n = 100$ bins are used to calculate the $\text{DEL}_t$ for the optimization problem. These

figures clearly illustrate how the reduction of the amplitude in $M_t$ results in the reduction of the $\text{DEL}_t$. The optimal solution $\boldsymbol{p}_{u,\text{opt}}$ reduces the fluctuations in $\omega_g$ as well, as shown in Fig. 9. Since $\tau_g$ is held constant in the above-rated region, this also leads to better tracking of $P$.

## 7 CONCLUSION

In this article, we present preliminary results for closed-loop, variable-pitch control of marine hydrokinetic turbines. ROSCO, an open-source tool developed by NREL, is used to derive the necessary controllers for a floating configuration of the Reference Model 1 (RM1) turbine. An optimization problem was formulated to identify the tuning parameters associated with the blade pitch controller to minimize the tower-base damage equivalent loading (DEL). The parameters identified by the controller result in a 20% reduction in the DEL. In future studies, the impact of minimizing the DEL on extending the lifetime and levelized cost of energy must be understood. The open-source tool WEIS is used to run the studies in this article. The approach and tools presented in this article can be used to design controllers for other axial-flow marine turbines as well.

Because of the computational cost associated with OpenFAST simulations, load cases from DLC 1.1 with a time span of 200 s were used in this study. The controller's and the turbine's performance must be tested for the multiple load cases and longer time horizons specified by the IEC [20]. The development of lower-order or surrogate models that can capture the dynamics of marine turbines and their use in control optimization must also be explored. These models could help in investigating the use of derivative-based or even global optimization solvers.

Even though the benefits of a blade pitch controller in the above-rated region have been established for marine turbines, fixed-pitch variable-speed control is still prevalent in the industry. For specific applications, the cost benefits of fixed-pitch turbines may outweigh the drawbacks. For such cases, a detailed comparison of the benefits of fixed-pitch and variable-pitch designs must be explored.

**TABLE 1**: Optimization results.

| Variable | Initial Value ($\boldsymbol{p}_{u,\text{init}}$) | Optimal Value ($\boldsymbol{p}_{u,\text{opt}}$) |
|---|---|---|
| $\omega_{\text{pc}}$ [rad/s] | $[0.90, 0.90]$ | $[0.40, 1.50]$ |
| $\zeta_{\text{pc}}$ [-] | $[0.70, 0.70]$ | $[1.09, 1.79]$ |
| $k_{\beta,\text{float}}$ [-] | $-0.38$ | $-0.76$ |
| $\omega_{\text{ptfm}}$ [rad/s] | 0.66 | 0.53 |
| $\text{DEL}_t$ [kNm] | 1327.89 | 1052.01 |
| $\omega_g$ overspeed [%] | 35.40 | 19.55 |


## ACKNOWLEDGMENT

This work was authored in part by the National Renewable Energy Laboratory, operated by Alliance for Sustainable Energy, LLC, for the U.S. Department of Energy (DOE) under Contract No. DE-AC36-08GO28308. Funding is provided by the U.S. Department of Energy Office of Energy Efficiency and Renewable Energy Water Power Technologies Office. The views expressed in the article do not necessarily represent the views of the DOE or the U.S. Government. The U.S. Government retains, and the publisher, by accepting the article for publication, acknowledges that the U.S. Government retains a nonexclusive, paid-up, irrevocable, worldwide license to publish or reproduce the published form of this work or allow others to do so for the U.S. Government purposes.


## References


[1] Garcia-Sanz, M., 2019. "A metric space with LCOE isolines for research guidance in wind and hydrokinetic energy systems". *Wind Energy,* ***23***(2), Nov., pp. 291–311. doi: 10.1002/we.2429

[2] Bir, G. S., et al., 2011. "Structural design of a horizontal-axis tidal current turbine composite blade". In Volume 5: Ocean Space Utilization; Ocean Renewable Energy, OMAE. doi: 10.1115/omae2011-50063

[3] Kilcher, L., et al., 2021. *Marine Energy in the United States: An Overview of Opportunities*. Feb. doi: 10.2172/1766861

[4] Salmon, A., et al., 2022. "Igiugig's journey towards sustainability". https://www.osti.gov/biblio/1903772.

[5] Jiang, B., et al., 2022. "Control co-design of a hydrokinetic turbine with open-loop optimal control". In Volume 8: Ocean Renewable Energy, OMAE. doi: 10.1115/omae2022-81006

[6] Ross, H., et al., 2023. "Development of a control co-design modeling tool for marine hydrokinetic turbines". In IMECE. doi: 10.1115/imece2022-94483

[7] Neary, V. S., et al., 2014. Methodology for design and economic analysis of marine energy conversion (MEC) technologies. Tech. rep., Mar. https://energy.sandia.gov/wp-content/gallery/uploads/SAND2014-9040-RMP-REPORT.pdf.

[8] Guo, X., et al., 2018. "Dynamic responses of a floating tidal turbine with 6-DOF prescribed floater motions". *Ocean Eng.,* ***165***, Oct., pp. 426–437. doi: 10.1016/j.oceaneng.2018.07.017

[9] Zhang, L., et al., 2015. "The effects of surge motion of the floating platform on hydrodynamics performance of horizontal-axis tidal current turbine". *Renew. Energy,* ***74***, Feb., pp. 796–802. doi: 10.1016/j.renene.2014.09.002

[10] Dewhurst, T., et al., 2013. "Dynamics of a floating platform mounting a hydrokinetic turbine". *Mar. Technol. Soc. J.,* ***47***(4), July, pp. 45–56. doi: 10.4031/mtsj.47.4.13

[11] de Jesus Henriques, T., et al., 2014. "The effects of wave–current interaction on the performance of a model horizontal axis tidal turbine". *Int. J. Mar. Energy,* ***8***, Dec., pp. 17–35. doi: 10.1016/j.ijome.2014.10.002

[12] Martinez, R., et al., 2020. "Analysis of the effects of control strategies and wave climates on the loading and performance of a laboratory scale horizontal axis tidal turbine". *Ocean Eng.,* ***212***, Sept., p. 107713. doi: 10.1016/j.oceaneng.2020.107713

[13] Tatum, S., et al., 2016. "Wave–current interaction effects on tidal stream turbine performance and loading characteristics". *Int. J. Mar. Energy,* ***14***, June, pp. 161–179. doi: 10.1016/j.ijome.2015.09.002

[14] Ordonez-Sanchez, S., et al., 2019. "Analysis of a horizontal-axis tidal turbine performance in the presence of regular and irregular

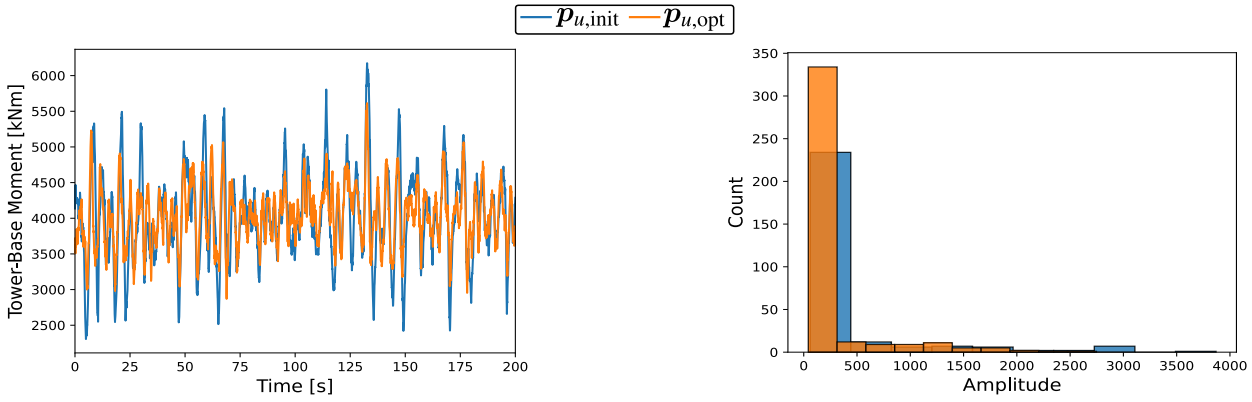


(a) Tower-base moment.

(b) Histogram plot of the amplitude for different cycles.

**FIGURE 8**: The time series plot for the tower-base moment ($M_t$), and the histogram plot of the amplitudes for the different cycles obtained using the rainflow counting method for $n = 10$ bins for $v_{\text{avg}} = 2.75$ m/s for both $\boldsymbol{p}_{u,\text{init}}$ and $\boldsymbol{p}_{u,\text{opt}}$.

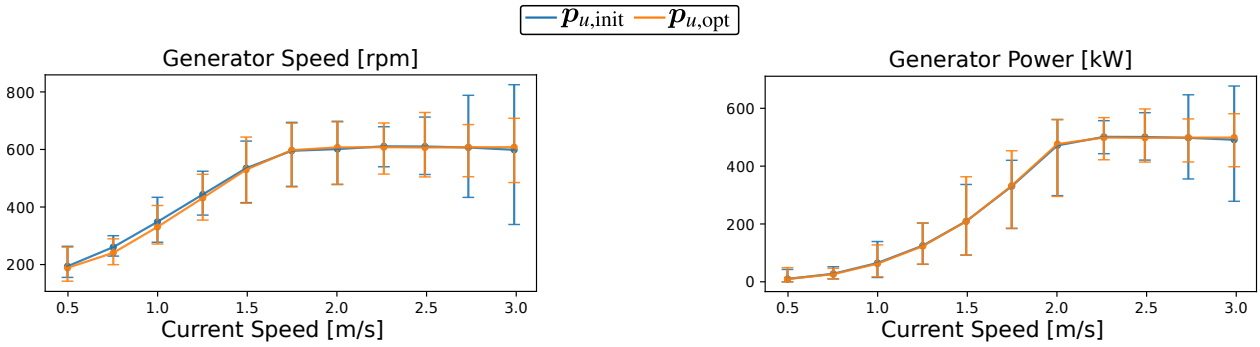


(a) Generator speed.

(b) Generator power.

**FIGURE 9**: The mean value and range of the generator speed ($\omega_g$) and generator power ($P$) for all 11 load cases for both $\boldsymbol{p}_{u,\text{init}}$ and $\boldsymbol{p}_{u,\text{opt}}$.


waves using two control strategies". *Energies,* ***12***(3), Jan., p. 367. doi: 10.3390/en12030367

[15] Whitby, B., and Ugalde-Loo, C. E., 2014. "Performance of pitch and stall regulated tidal stream turbines". *IEEE Trans. Sustain. Energy,* ***5***(1), Jan., pp. 64–72. doi: 10.1109/tste.2013.2272653

[16] Pao, L. Y., and Johnson, K. E., 2009. "A tutorial on the dynamics and control of wind turbines and wind farms". In American Control Conference. doi: 10.1109/acc.2009.5160195

[17] Gunnink, T., 2015. "Analysis and regulation of the coupled dynamics of a two- turbine floating tidal energy converter". M.S. Thesis, Delft University of Technology, Delft, NL, Aug. http://resolver.tudelft.nl/uuid:4670bb38-ffbb-44c1-86ac-0d6498d9433f.

[18] Zalkind, D., et al., 2020. "Automatic controller tuning using a zeroth-order optimization algorithm". *Wind Energy Sci.,* ***5***(4), Nov., pp. 1579–1600. doi: 10.5194/wes-5-1579-2020

[19] Zalkind, D., et al., 2019. "System-level design studies for large rotors". *Wind Energy Sci.,* ***4***(4), Nov., pp. 595–618. doi: 10.5194/wes-4-595-2019

[20] IEC, 2019. Marine energy - wave, tidal and other water current converters - part 2: Marine energy systems - design requirements. Tech. rep., Oct.

[21] Zalkind, D., et al., 2022. "Floating wind turbine control optimization". *J. Phys. Conf. Ser.,* ***2265***(4), May, p. 042021. doi: 10.1088/1742-6596/2265/4/042021

[22] Murray, R. E., et al., 2018. "Added-mass effects on a horizontal-axis tidal turbine using FAST v8". *Renew. Energy,* ***126***, Oct., pp. 987–1002. doi: 10.1016/j.renene.2018.04.023

[23] Abbas, N. J., et al., 2022. "A reference open-source controller for fixed and floating offshore wind turbines". *Wind Energy Sci.,* ***7***(1), Apr., pp. 53–73. doi: 10.5194/wes-7-53-2022

[24] Wiley, W., et al., 2023. "Design and modeling of an open-source baseline floating marine turbine". In UMERC. https://www.nrel.gov/docs/fy24osti/87249.pdf.

[25] Qian, P., et al., 2019. "Review on configuration and control methods of tidal current turbines". *Renew. Sustain. Energy Rev.,* ***108***, July, pp. 125–139. doi: 10.1016/j.rser.2019.03.051

[26] Gu, Y.-J., et al., 2018. "Blade-pitch system for tidal current turbines with reduced variation pitch control strategy based on tidal current velocity preview". *Renew. Energy,* ***115***, Jan., pp. 149–158. doi: 10.1016/j.renene.2017.07.034

[27] García, E., et al., 2022. "Control and supervision requirements for floating hybrid generator systems". *Int. J. Environ. Res. Public Health,* ***19***(19), Oct., p. 12781. doi: 10.3390/ijerph191912781

[28] Ness, K. V., et al., 2021. "Experimental comparison of blade pitch

and speed control strategies for horizontal-axis current turbines". *J. Ocean Eng. Mar. Energy,* ***7***(1), Feb., pp. 83–96. doi: 10.1007/s40722-021-00188-w

[29] Gracie-Orr, K., et al., 2016. "Development and initial application of a blade design methodology for overspeed power-regulated tidal turbines". *Int. J. Mar. Energy,* ***15***, Sept., pp. 140–155. doi: 10.1016/j.ijome.2016.04.006

[30] Djebarri, S., et al., 2015. "Influence of fixed-pitch tidal turbine hydrodynamic characteristic on the generator design". In European Wave and Tidal Energy Conference. https://api.semanticscholar.org/CorpusID:112395408.

[31] Arnold, M., et al., 2016. "Load reduction potential of variable speed control approaches for fixed pitch tidal current turbines". *Int. J. Mar. Energy,* ***15***, Sept., pp. 175–190. doi: 10.1016/j.ijome.2016.04.012

[32] Jonkman, J., 2008. "Influence of control on the pitch damping of a floating wind turbine". In 46th AIAA Aerospace Sciences Meeting and Exhibit. doi: 10.2514/6.2008-1306

[33] OpenFAST. [Online, 48b0ae6]. url: https://github.com/OpenFAST/openfast/tree/dev

[34] ROSCO. [Online, 989ce5b]. url: https://github.com/NREL/ROSCO/tree/develop

[35] Franklin, G. F., Powell, J. D., and Emami-Naeini, A., 2015. *Feedback control of dynamic systems*, Vol. 33. Pearson London.

[36] van der Veen, G. J., et al., 2012. "Control of floating wind turbines". In American Control Conference. doi: 10.1109/acc.2012.6315120

[37] Larsen, T. J., and Hanson, T. D., 2007. "A method to avoid negative damped low frequent tower vibrations for a floating, pitch controlled wind turbine". *J. Phys. Conf. Ser.,* ***75***, July, p. 012073. doi: 10.1088/1742-6596/75/1/012073

[38] Wang, T., and Yang, Z., 2020. "A tidal hydrodynamic model for cook inlet, alaska, to support tidal energy resource characterization". *J. Mar. Sci. Eng.,* ***8***(4), Apr., p. 254. doi: 10.3390/jmse8040254

[39] Natarajan, A., 2022. "Damage equivalent load synthesis and stochastic extrapolation for fatigue life validation". *Wind Energy Sci.,* ***7***(3), June, pp. 1171–1181. doi: 10.5194/wes-7-1171-2022

[40] Amzallag, C., et al., 1994. "Standardization of the rainflow counting method for fatigue analysis". *Int. J. Fatigue,* ***16***(4), June, pp. 287–293. doi: 10.1016/0142-1123(94)90343-3

[41] Freebury, G., and Musial, W., 2000. "Determining equivalent damage loading for full-scale wind turbine blade fatigue tests". In ASME Wind Energy Symposium. doi: 10.2514/6.2000-50

[42] Miao, Y., et al., 2022. "A machine learning method for modeling wind farm fatigue load". *Appl. Sci.,* ***12***(15), July, p. 7392. doi: 10.3390/app12157392

[43] Powell, M. J. D., 1994. "A direct search optimization method that models the objective and constraint functions by linear interpolation". In *Advances in Optimization and Numerical Analysis*. Springer Netherlands, pp. 51–67. doi: 10.1007/978-94-015-8330-5_4

[44] WEIS. [Online, 9489f4f]. url: https://github.com/WISDEM/WEIS/tree/ct-opt